Full-spectrum volumetric solar thermal conversion via graphene/silver hybrid plasmonic nanofluids

Mehrali, Mohammad; Ghatkesar, Murali Krishna; Pecnik, Rene

DOI
10.1016/j.apenergy.2018.04.065

Publication date
2018

Document Version
Final published version

Published in
Applied Energy

Applied Energy 224 (2018) 103–115

Contents lists available at ScienceDirect

Applied Energy

journal homepage: www.elsevier.com/locate/apenergy

Full-spectrum volumetric solar thermal conversion via graphene/silver hybrid plasmonic nanofluids

Mohammad Mehrali[a,*], Murali Krishna Ghatkesar[b], Rene Pecnik[a,1]

[a] Process and Energy Department, Delft University of Technology, Leeghwaterstraat 39, 2628CB Delft, The Netherlands
[b] Department of Precision and Microsystems Engineering, Delft University of Technology, Mekelweg 2, 2628 CD Delft, The Netherlands

HIGHLIGHTS

- Hybrid plasmonic nanofluids containing Ag decorated rGO have been prepared.
- The photo-thermal potency promoted by the synergistic effects between rGO and Ag nanoparticles.
- The hybrid nanofluid can realize both higher absorption feature and thermal conductance.
- A collector efficiency of 77% is achievable for low concentration of nanofluids.

GRAPHICAL ABSTRACT

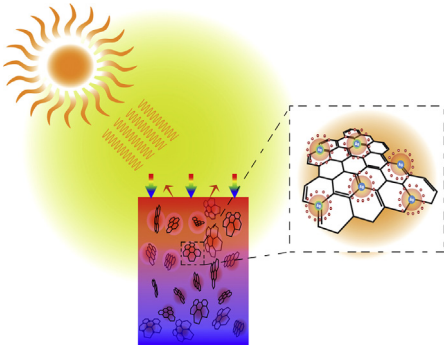

ARTICLE INFO

Keywords:
Plasmonic nanofluid
Solar absorption
Graphene nanofluid
Optical properties
Direct absorption solar collectors

ABSTRACT

The wide-spread adoption of solar thermal absorbers is currently hampered by their low absorption efficiencies and their high capital cost. As a result, a number of initiatives, including direct absorption solar collectors (DASC), are currently underway to improve the absorber efficiencies. In this regard, this study focused on application of hybrid nanofluids containing reduced graphene oxides decorated with silver nanoparticles in volumetric solar absorbers. Their superior solar absorptance and thermal conductivity is based on the plasmonic effect of the nanoparticles and high thermal conductivity of graphene nanosheets, respectively. Several parameters such as mass concentration of graphene nanosheets and Ag decoration contents were studied that could affect the thermal and optical properties of the nanofluids. The results indicated that the prepared nanofluids can be employed for direct absorption solar collectors over a short period of solar irradiation time, even at a low illumination intensity of one sun. A collector efficiency of 77% is achievable at low concentration of 40 ppm owing to the enhanced light absorption of graphene at the excitation wavelength. These findings therefore suggest that this solution can contribute to the final goal of utilizing nanofluids for efficient solar thermal energy harvesting.

1. Introduction

A vast use of photovoltaic, concentrated solar power and solar thermal technologies is anticipated to play a decisive role in the future energy landscape, considering that the conversion of solar energy becomes more efficient and cost-effective [1]. As such, a significant

* Corresponding author.
E-mail addresses: M.Mehrali@tudelft.nl (M. Mehrali), r.pecnik@tudelft.nl (R. Pecnik).
[1] Principal corresponding author.

https://doi.org/10.1016/j.apenergy.2018.04.065
Received 7 February 2018; Received in revised form 7 April 2018; Accepted 26 April 2018

technological improvement must be achieved for solar thermal collectors in heating and cooling applications of industrial, commercial, residential and service sectors. In conventional solar thermal collectors, the solar irradiance heats up an absorber surface using a selective coating and heat is transferred to the working fluid driven by a temperature difference [2]. In typical configurations, the conductive and convective thermal resistances between the absorber and the fluid makes the effectiveness of the solar-to-thermal energy conversion quite limited, because of high heat losses from the surface absorber to the surroundings [3]. In view of this shortage, direct volumetric receivers or absorbers, also named as direct absorption solar collectors (DASCs), have been proposed and considered as a promising alternative for further improving the thermal efficiency [4,5]. Depending on the application, various potential working fluids have been proposed for DASC systems including water, ethylene glycol, water/ethylene glycol mixtures and a wide range of oils. However, their low solar radiation absorption does not allow high solar thermal efficiencies in various applications [6].

Nanofluids that contain nanoparticles which efficiently absorb solar radiation promise to overcome these difficulties in photo-thermal solar energy conversion. Notably, their superior optical and thermo-physical properties, including thermal conductivity, play a key role to enhance solar energy absorption and conversion [7]. A series of studies have been performed in order to optimize solar absorption of nanofluids, with respect to nanoparticle material, size, shape, volume fraction, etc. The materials used can be pure metals (Au [8–10], Ag [11,12], Cu [13] and Al [14]), metal oxides (Al_2O_3 [15], CuO [16,17], Fe_3O_4 [18], SiO_2 [19] and TiO_2 [20]), carbides (SiC [21], TiC [22]) and different types of carbon materials (graphite [23], such as single/multi wall carbon nanotubes [24–26] and graphene [27,28]). The outcome of these studies are presented in Table 1, which confirm the capability of nanofluids to enhance the efficiency of DASC systems.

In previous work, a series of investigations showed that nanoparticles clearly offer the potential to improve the solar absorption if they are dispersed in the heat transfer fluid. For example, the absorption of solar radiation can be enhanced at a certain wavelength by a phenomena called localized surface plasmon resonance (LSPR). This phenomena takes place when the collective oscillation frequency of free electrons of the nanoparticle resonates with the incident light [31]. The local electric field in the vicinity of the nanoparticle is then greatly enhanced, which leads to a significant increase of solar radiation absorption and scattering. The effect of surface plasmon resonance (SPR) that mostly occurs in the visible light spectrum contains approximately 40% of the total solar energy [32]. Zhang et al. [33] demonstrated that using 116 mg/L aqueous gold nanofluid could enhance the photothermal conversion efficiency by 80% and reached a specific absorption rate (SAR) of ~1 kW/g under a solar simulator. Amjad et al. [34] and Wang et al. [35] investigated the absorption of aqueous gold nanofluids for direct solar steam generation. The highest evaporation efficiency (40%) was achieved under 10 Suns irradiation by a 178 ppm aqueous gold nanofluid, which however might not be economically feasible due to the high cost of gold. An enhancement of 144% in the photothermal conversion efficiency and specific absorption rate of 0.6 kW/g were achieved by using 68 mg/L silver aqueous nanofluid in outdoor conditions [36]. The enhancement of absorption for plasmonic nanofluids has unavoidably a narrow bandwidth owing to their resonance characteristic [37]. As a result, the particle concentration may have to be increased to make up for the weak absorption outside the plasmonic resonance spectrum. However, a higher particle concentration will increase the cost of the nanofluid and lead to technical challenges, such as an increased fluid viscosity and wear of pipings. Therefore, achieving a broadband, especially full-spectrum, volumetric solar thermal absorption is still a daunting challenge [6].

To achieve a broadband absorption, hybrid nanofluids were suggested by some researchers. Lee et al. [36] predicted the absorption coefficient of nanofluids embedded with SiO_2-Au core-shell nanoparticles and showed an efficiency of 70% was achieved by 0.05 vol% of hybrid nanofluid. Liu et al. [38] synthesized SiO_2/Ag particles with different thicknesses of silver shells, and the extinction peaks of SiO_2/Ag particles shifted from visible to the near-infrared region. Zeng et al. [39] investigated binary CNT-SiO_2/Ag nanofluids for solar-thermal conversion applications. The results indicated that binary nanofluids containing 0.1 vol% nanomaterials, reached the highest instantaneous photo-thermal conversion efficiency, which was 80% at ~40 °C. However, although the tunability of the optical properties of such core-shell nanoparticles is achievable, the difficulty in manufacturing this type of nanoparticles makes it less suitable for large scale solar applications. A fair comparison of the photothermal performance under a given concentration between the hybrid and its original nanofluids is still lacking. Such a comparison is crucial to check the feasibility of hybrid nanofluids.

Moreover, in most of the previous studies, a uniform temperature distribution within a nanofluid was assumed, although the effect of the optical path was not negligible, and one temperature was used to calculate the photothermal conversion efficiency [40]. However, the nonlinear reduction in the radiative intensity along the depth of the nanofluid should cause a temperature difference within the nanofluid. Neglecting this temperature difference would lead to an inaccurate calculation of the efficiency. In addition to the efficiency, the cost has to be considered carefully for any practical applications.

Owing to its unique and superior optical, electronic and thermal properties, two-dimensional (2D) graphene has been used in many fields, including photo-thermal nanofluids in solar energy applications [41]. Graphene nanosheets have a higher thermal conductivity than

Table 1
The solar-thermal performance of the selected nanofluid-based direct absorption solar collector.

Nanoparticle	Working fluid	Fraction	Major result of the study	Ref.
Au	Distilled water	0.5–2.5 ppm	The absorption efficiency increased exponentially with increasing collector height and nanoparticles volume fraction	[8]
Ag	Distilled water	6.2 ppm	The collector efficiency enhanced at higher collector height and nanoparticles volume fraction	[11]
Cu	Distilled water	1–7 vol%	Collector efficiency increased more than 2 times compared with that of base fluid	[13]
Al	Distilled water	1–5 vol%	Efficiency remarkably increased for volume fraction less than 2% and it remained nearly constant at higher volume fractions	[14]
Al_2O_3	Distilled water + Triton X-100	0.2–0.4 wt%	Collector efficiency at 0.2 wt% was enhanced 28.3% compared with that of water and dropped to 15.63% by adding surfactants	[29]
CuO	Water/ethylene glycol	12.5–100 ppm	Absorbed energy fraction of CuO nanofluid was 4 times higher than that of base fluid	[17]
Fe_3O_4	Deionized water	5–40 ppm	The collector thermal efficiency enhancement was 57.4% at concentration of 40 ppm	[18]
TiO_2	Distilled water	0.03–0.08 vol%	An increase of up to 61% transmissivity was noted for 0.08% volume fraction	[20]
SiC	[HMIM]BF4	0.01–0.06 wt%	The transmittance of 0.03 wt% SiC nanofluids dropped to zero on the whole wavelength range	[21]
Graphite	(BMIM) BF4	0.01 wt%	An efficiency enhancement of 9.4–10.7% was observed	[30]
CNT	Deionized water	5.6–53 mg/ml	An Optical characterization of the nanofluids demonstrated that the MWCNTs were highly absorbing over the majority of solar spectrum	[25]
Graphene	[HMIM]BF4	0.0005–0.001 wt%	The maximum receiver efficiency enhancement was 70%	[27]

other nanoparticles, due to their large intrinsic thermal conductivity, and low density when compared to metal or metal oxides [42]. In the previous studies in which plasmonic nanofluids or grapehen nanofluids were involved, the light absorption property was limited because of using unitary nanofluids. Therefore, this study proposed to combine the advantages of both metal nanoparticles and graphene, which expected to improve solar radiation harvesting and enhance the overall efficiency of low-temperature DASCs. Recently, Ag-graphene composites have been developed and applied in the fields of photocatalysis, surface enhanced Raman scattering, sensors, conductive transparent electrodes, fuel cells and photocurrent generation. It is believed that the hybridization of graphene with Ag can result in better properties that are superior to individual Ag nanoparticles themselves. There are many studies that have investigated solar energy trapping and conversion of Ag or graphene based nanofluids separately [43], while there are no studies focusing on photothermal effects of Ag decorated graphene nanofluids for low-temperature DASCs.

This study aims to overcome the issues reviewed above and perform a well-controlled experiment for hybrid plasmonic nanofluids that can be used for volumetric solar collectors. In this work, a facile, convenient, and low-cost method was used to synthesize highly water-dispersible silver decorated reduced graphene oxide (Ag-rGO) composites. The dispersion stability, thermal conductivity and viscosity of the prepared suspensions were characterized for bare rGO nanofluids and Ag-rGO nanofluids with various Ag contents. The radiative properties of Ag-rGO nanofluids have been investigated experimentally for the first time by varying the weight fraction, and the optical path length. Finally, the solar photo-thermal conversion efficiency of Ag-rGO nanofluids is discussed to evaluate the potential of using these nanofluids for absorbing solar radiation in volumetric solar absorbers. This work advances the understanding of plasmonic graphene based nanofluids, which promises to be a low-cost option with potential application for DASCs systems.

2. Material synthesis and experimental methods

2.1. Nanofluid synthesis and preparation

Graphene oxide (GO) nanosheets were synthesized trough an oxidation process of graphite flakes by following the modified Hummers method [44]. The silver decorated reduced graphene oxides (Ag-rGO) were prepared by means of the straightforward wet-chemical method. In this method, the Ag-rGO nanosheets are prepared in a DMF solution, where DMF acts simultaneously as a solvent and a reducing agent. A co-reduction technique has been employed for both GO and $AgNO_3$ with DMF at ~ 80 °C. In this procedure, Ag^+ is reduced to Ag^0 with DMF and afterwards DMF self-oxidizes to dimethylcarbamic acid [$(CH_3)_2NCOOH$], along with restoring the electronic conjugation within the graphene sheets [45]. The schematic process of the synthesis is illustrated in Fig. 1.

The preparation of the nanofluids was as follows. First, 0.3 g of dried GO was sonicated in 200 mL of DMF (as reducing agent) for 1 h in a beaker. In another beaker, specific amounts of $AgNO_3$ (0.15 and 0.3 g) were stirred in 10 mL of deionized water for 5 min. An aqueous solution of $AgNO_3$ was then added into the above mentioned GO suspension, and the obtained mixture was further stirred and refluxed at 80 °C for 8 h. Finally, the black product was centrifuged and washed with ethanol and deionized water. The same procedure was repeated without adding $AgNO_3$ to prepare the bare rGO. The samples with 0.15 and 0.3 g of $AgNO_3$ were labeled as S1 and S2, respectively. Nanofluids with different concentrations (10, 20, 40, 80 and 100 ppm (mass per unit volume:10, 20, 40, 80 and 100 mg/L) were prepared by dispersing synthesized rGO and Ag-rGO nanosheets in deionized water, following bath sonication for 5 min. It is worth mentioning that Ag has a higher density compared with rGO which will affect the number of particles for the same concentrations in different nanofluids.

2.2. Instrumentations

Transmission electron microscopy (TEM) was performed using a JEOL (JEM1400) transmission electron microscope. SEM imaging was carried out with a JEOL (JSM-6010LA) scanning electron microscope. The X-ray diffraction (XRD) was conducted on a Bruker D2 Phaser XRPD. The elemental analysis was performed by X-ray Photoelectron Spectroscopy (XPS, PHI5600) with an Al-Kα monochromatic X-ray source (hν = 1486.71 eV). A Lambda35 UV–vis spectrometer was used to characterize the optical properties with wavelength accuracy of ±0.1 nm. The absorption spectra of the nanofluids were measured using a UV–vis-NIR (PerkinElmer, Lambda950) spectrophotometer with wavelength accuracy of ±0.1 nm. The viscosity of the nanofluids were measured at different temperatures using the rheometer (TA Instruments, Ar 2000 Ex) with maximum error of 4%. The thermal conductivity of the nanofluids for different Ag-rGO concentrations was measured with a C-Therm TCi thermal conductivity analyzer with accuracy of ±(3% + 0.02) W/m K. An infrared camera (FLIR SC325) was utilized to obtain the surface temperature distribution of the nanofluids with thermal sensitivity of ±0.1 °C.

2.3. Photo-thermal conversion experiment

A schematic of the photo-thermal experimental setup is shown in Fig. 2. The fabricated test section in the shape of a cylinder was made of polymethyl methacrylate (PMMA) with an inner diameter of 30 mm and a height of 20 mm. The cylinder was completely insulated to reduce heat losses from the collector walls and the quartz window covering the top of the cylinder. For evaluating the temperature distribution of the nanofluid, five K-type thermocouples were installed in the center of cylinder at different heights (y/h = 0.2, 0.4, 0.6, 0.8 and 1) and connected to a data logging unit (Omega-TC08) to transfer the readings to a computer. An artificial sunlight simulator (WACOM-WXS-90S) was used as a light source with the capability of one sun irradiance that meets class AAA standard and an AM1.5 spectrum. The intensity of the simulated light was measured with a pyranometer (KIPPZONEN-SMP21) during the duration of the experiment, in order to calculate an average value for further consideration. The uncertainty of the measured temperatures was evaluated to be ±0.1 °C.

3. Nanofluid characterization

3.1. Material morphology

The TEM images of the Ag-rGO samples, S1 and S2, are shown in Fig. 3(a) and (b), respectively. The impact of varying the amount of silver nitrate can be clearly seen in the TEM images, which confirms the monotonic distribution of Ag nanoparticles on the surface of the rGO sheets. The decorated Ag nanoparticles are spherical, having a mean particle size of 25–45 nm. The influence of the Ag decoration on the morphology of the rGO nanosheets is indicated by comparing the SEM images of the rGO and S2 samples in Fig. 3(c) and (d). The rGO has a wrinkled sheet microstructure, while tiny Ag nanoparticles are uniformly anchored on its surface after the decoration process.

3.2. Material composition

Fig. 4(a) shows the X-ray diffraction pattern of GO, rGO, S1 and S2 samples. The main peak of GO at $2\Theta = 10.5^{\circ}$ corresponds to the (001) plane, which is much higher than for graphite, confirming the vast exfoliation of graphite. On the other hand, this peak shifts to $2\Theta = 23.6^{\circ}$ for rGO, S1 and S2, indicating the extensive elimination of functional groups during the reduction process and restored graphitic moiety. The XRD patterns of the Ag-rGO samples have five major peaks that can be indexed to its (111), (200), (220), (311) and (222) crystallographic planes of Ag (JCPDS No. 04-0783). This confirms the

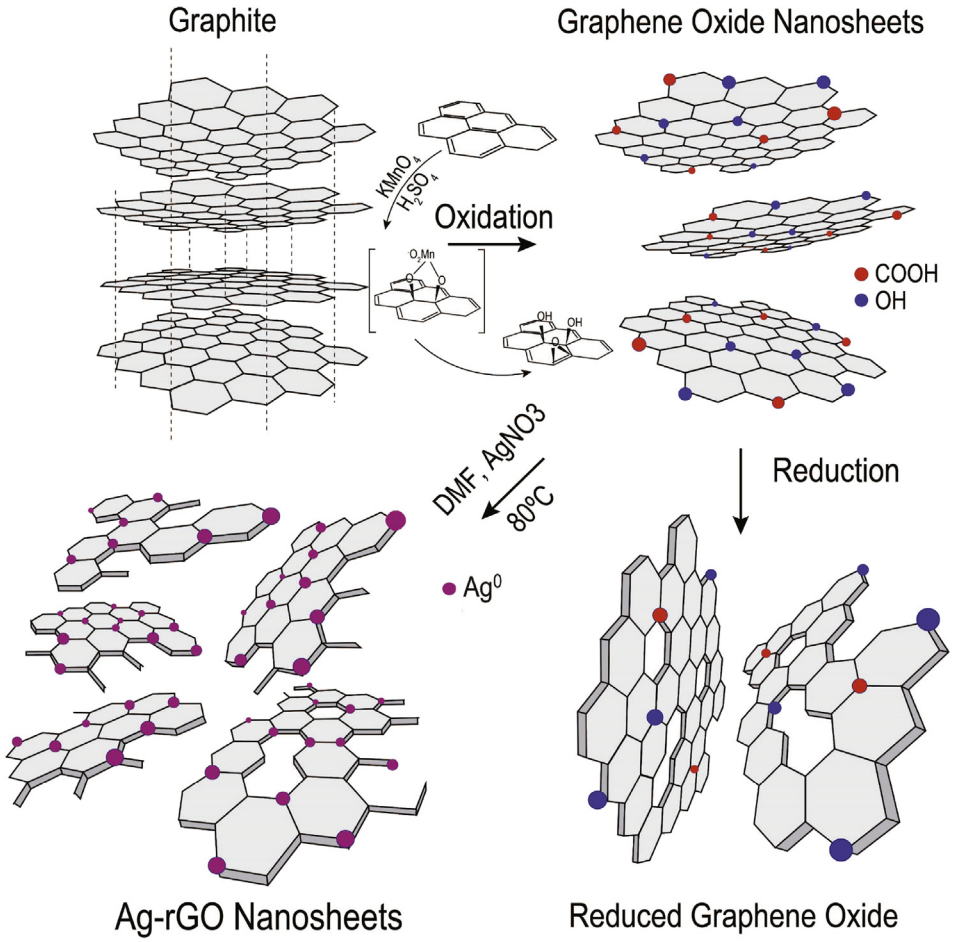

Fig. 1. Schematic of the formation of rGO and Ag-rGO nanosheets using the catalytic DMF.

presence of a cubic Ag nanoparticle phase.

The XPS spectroscopy was used to evaluate the relative elemental compositions of the prepared materials, which are shown in Fig. 4(b). The increment of the C/O ratio and the attenuated peaks of oxygen (O1s) indicate that GO was reduced efficiently. In particular, the C/O ratio in S2 is higher than S1, suggesting that the Ag decoration assists the reduction process of GO, while more Ag nanoparticles were decorated as confirmed by the atomic percentages presented in Table S1. The C1s spectrum of GO (Fig. S1(a)), rGO (Fig. S1(b)), and S2 (Fig. 4(c)) has four major Gaussian curves centered at binding energies of 284.17, 286.2, 288.1 and 290.2 eV that correspond to C=C/C–C, C–O, C=O, and O=C–O oxygen and carbon containing bonds, respectively [46]. The differences between these spectrums affirm the deoxygenation and reduction of GO in presence of DMF at 80 °C. Fig. 4(d) shows a narrow scan of the Ag3d doublet, which consist of binding energies of Ag $3d_{5/2}$ and Ag $3d_{3/2}$ electronic states separated by 6.0 eV in binding energy, which indicates the existence of Ag^0 in the Ag-rGO composite materials.

3.3. Thermal stability and macroscopic transport properties

Fig. 5(a) shows the UV–vis absorption spectra, used to evaluate the stability of the nanofluid, of the GO, rGO and Ag-rGO aqueous

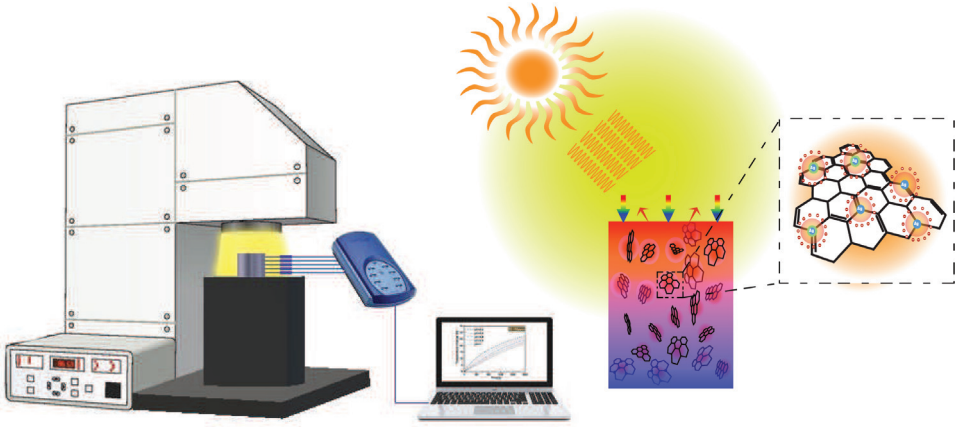

Fig. 2. Schematic of the experimental setup.

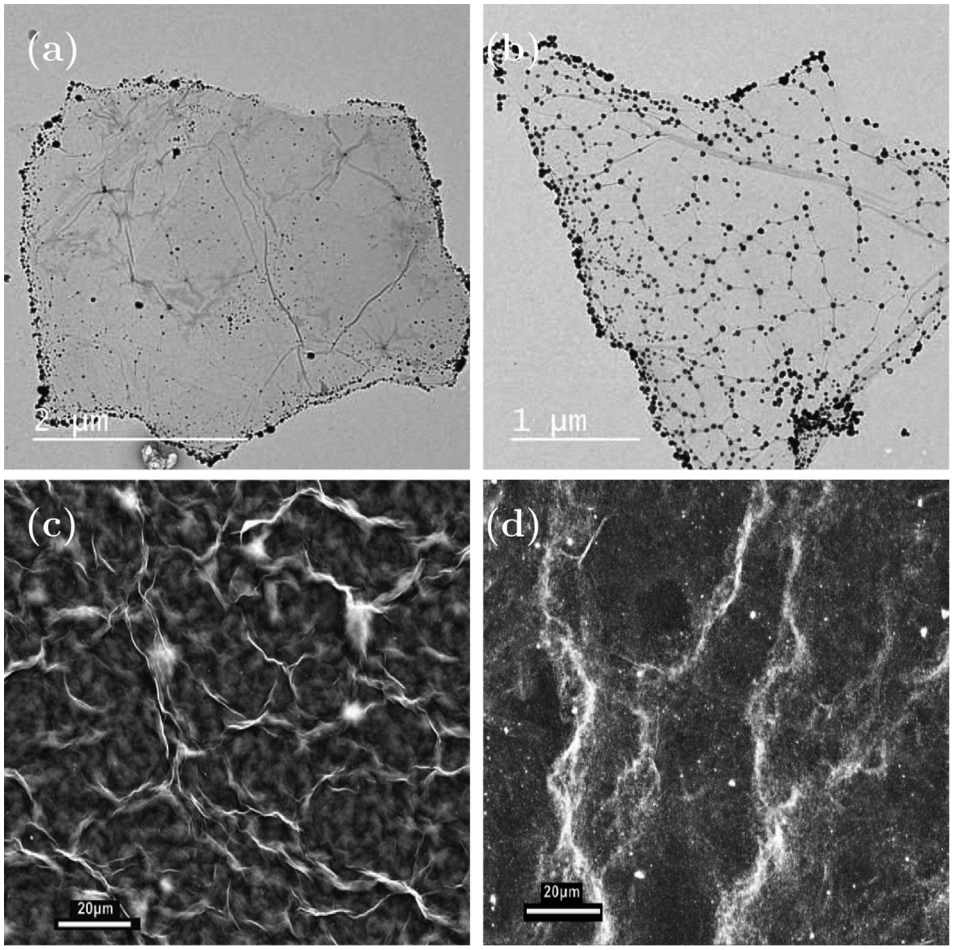

Fig. 3. TEM images of (a) S1, (b) S2; FESEM images of (c) rGO, (d) Ag-rGO.

nanofluids. The sharp peak of GO can be attributed to a $\pi-\pi^*$ transition (~228 nm). This peak is red-shifted to 270 nm for rGO, S1 and S2, which confirms the restoration of conjugation during reduction [47]. On the other hand, if the rGO is decorated with the Ag nanoparticles, the relative absorbance increases and an additional broad peak appears around 420 nm. This additional peak is related to the optical signature of the plasmonic silver nanoparticles (anchored on the rGO nanosheets), which is caused by transverse electronic oscillations. This result shows a considerable increment in the absorbance of the Ag-rGO nanofluids in the visible range if compared to the rGO nanofluid.

The stability of nanofluids greatly affects their heat transfer proficiency. Hence, the sedimentation rate of the dispersed nanoparticles within the fluid (highest concentration of 100 ppm) was investigated over a period of 1000 h. For the present work, the absorbance of water was taken as reference and the measurement was performed at a certain time interval within 1000 h. The percentage of relative concentration was based on the ratio of subsequent weight concentration of the sample to that of the fresh sample. The result in Fig. 5(b) shows that the nanofluids rGO, S1 and S2 are stable up to 7 days, while the maximum sedimentation of around 16% was reached after 1000 h for S2.

The viscosity of the nanofluids plays an important role in considering pumping power in practical applications of solar energy receivers. Thus, the relative viscosity of the nanofluids (μ_{nf}/μ_{water}) at their highest concentrations (100 ppm) were quantified for a temperature range of 25–60 °C, shown in Fig. 5(c). The maximum relative viscosity for all nanofluids occurs at the same temperature of 60 °C. The relative viscosity of all fluids increases nonlinearly with temperature, while the rGO nanofluid indicates the highest viscosity enhancement of 22% within the considered temperature range. The shearing flow resistance of prepared nanofluids demonstrated a similar trend as shown in Fig. 5(c). Moreover, the S1 and S2 nanofluids show a lower relative viscosity enhancement which is beneficial to decrease pumping power in energy systems. On the other hand, the relative viscosity increase for the prepared nanofluids at their highest concentration is less than the results of other nanoparticles based nanofluids [48].

The thermal conductivity enhancement of nanofluids is discussed as an enticing capability for solar energy systems. Thus, thermal conductivity ratio of prepared nanofluids (100 ppm) at different temperatures in the range of 15–40 °C are illustrated in Fig. 5(d). The maximum augmentation is observed at the highest temperature of 40 °C for rGO, S1 and S2 nanofluids, being 10%, 14% and 18%, respectively. Indeed, the Ag decoration can enhance the thermal conductivity of the rGO based nanofluids, which can be explained by the Ag deposition on the graphene edges that act as a thermal bridge between the nanosheets and the bulk fluid. In spite of this fact, increasing the Ag decoration, can increase the average density of the nanosheets, causing an overall lower number of nanosheets in nanofluids at the same mass concentration, which will reduce the thermal conductivity enhancement for the S2 samples. The combination of the Ag nanoparticles and the rGO nanosheets forms a strong interface network that supplies a percolation path for ballistic transfer of heat.

3.4. Solar absorption characteristics

The optical transmittance spectra (wavelength: 200–2500 nm) of the nanofluids have been measured at room temperature using quartz cuvettes and a 10 mm beam path length. The results are shown in Fig. 6. Water shows the well-known behaviour with an average transmittance

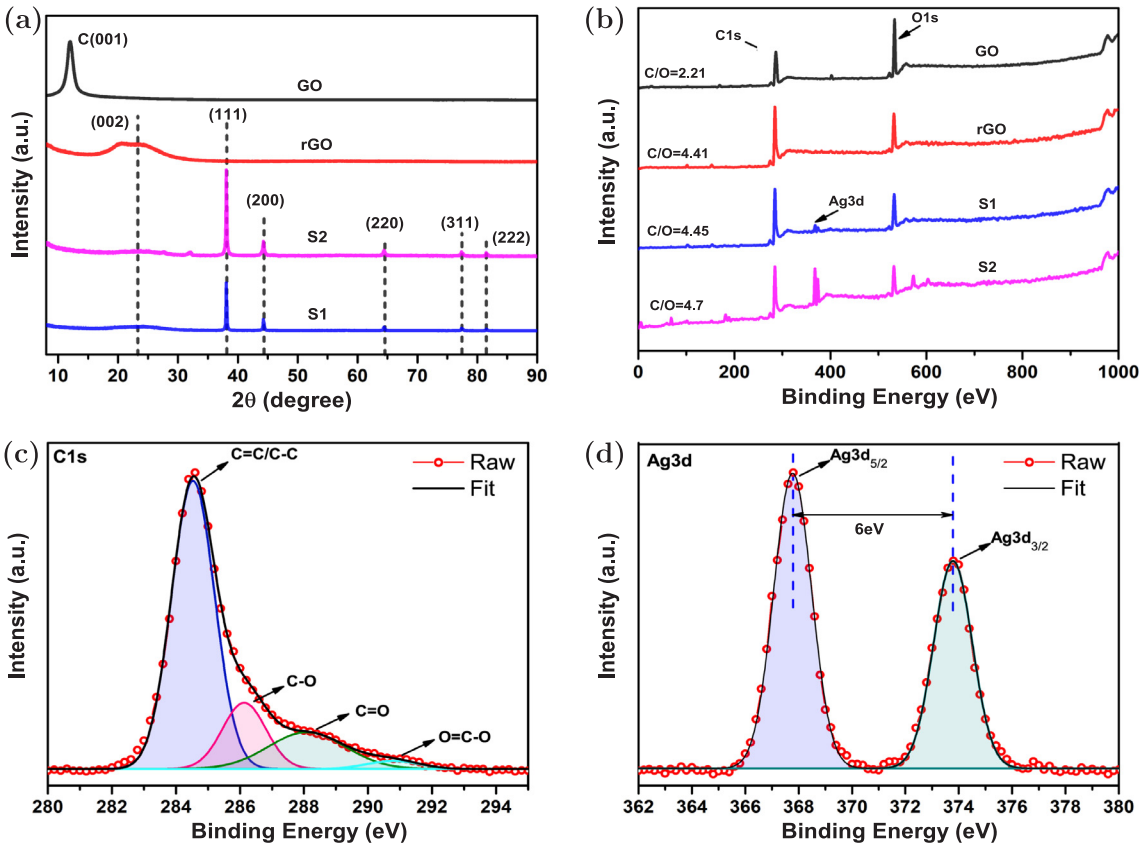

Fig. 4. (a) XRD spectra of GO, rGO, S1and S2; (b) XPS spectra of GO, rGO, S1and S2; (c) C1s spectra of S2; (d) Ag3d spectra of S2.

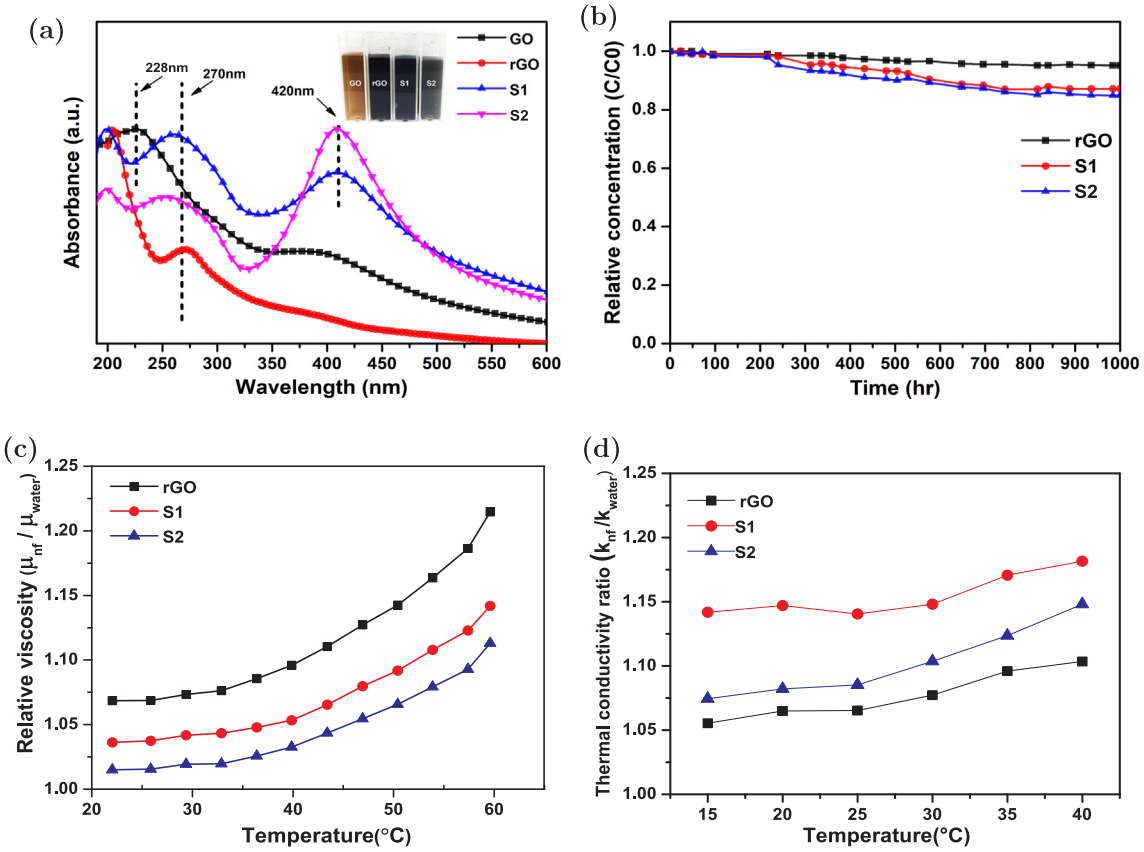

Fig. 5. (a) UV–vis absorption spectra of GO, rGO and Ag-rGo nanofluids; (b) sedimentation rate of nanofluids versus time; (c) relative viscosity (μ_{nf}/μ_{water}) and (d) thermal conductivity ratio(K_{nf}/k_{water}) as a function of temperature for nanofluids with a concentration of 100 ppm.

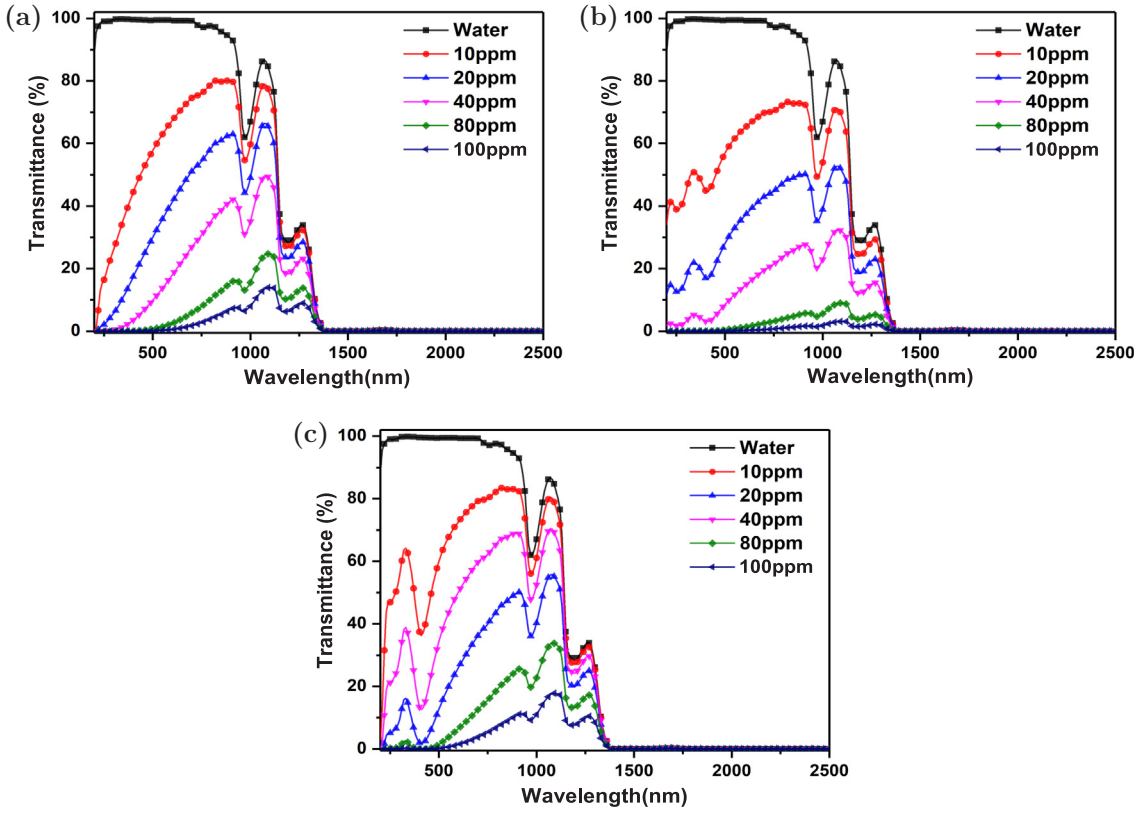

Fig. 6. Transmittance spectra of (a) rGO (b) S1 and (c) S2 nanofluids for different nanoparticle concentrations.

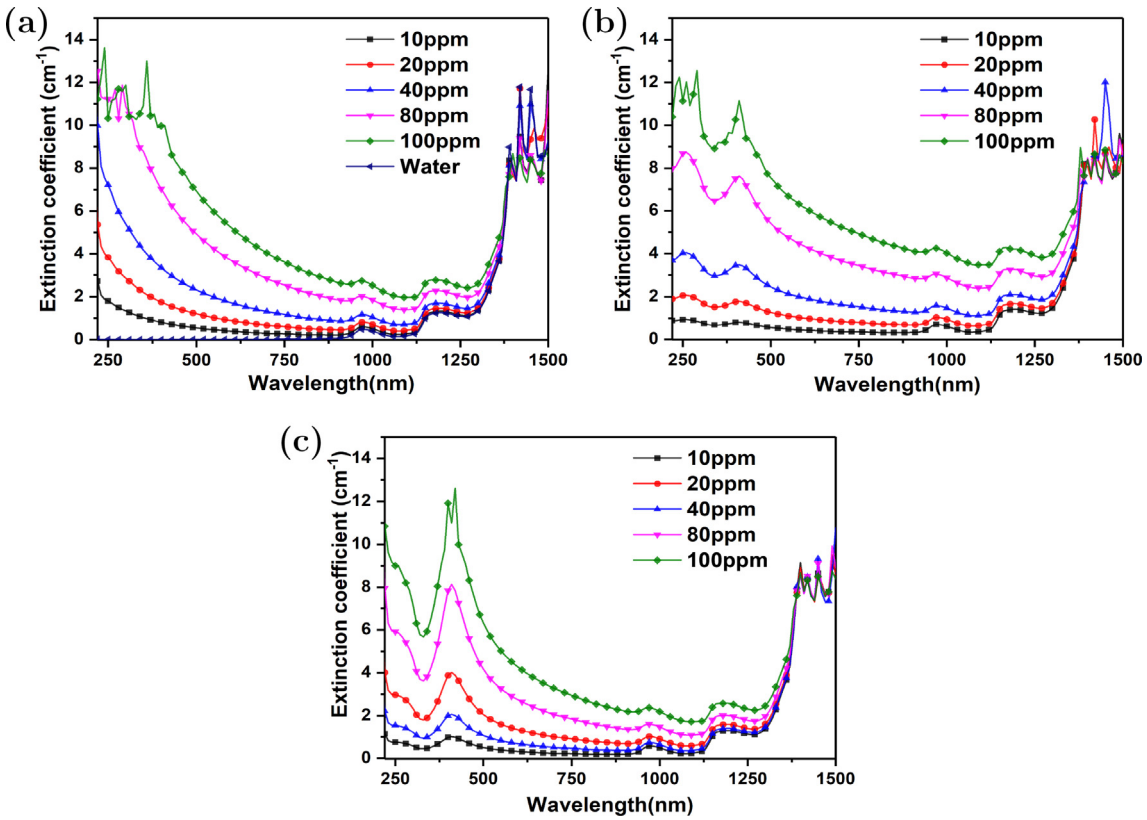

Fig. 7. Spectral extinction coefficient of (a) rGO (b) S1 and (c) S2 nanofluids for different nanoparticle concentrations.

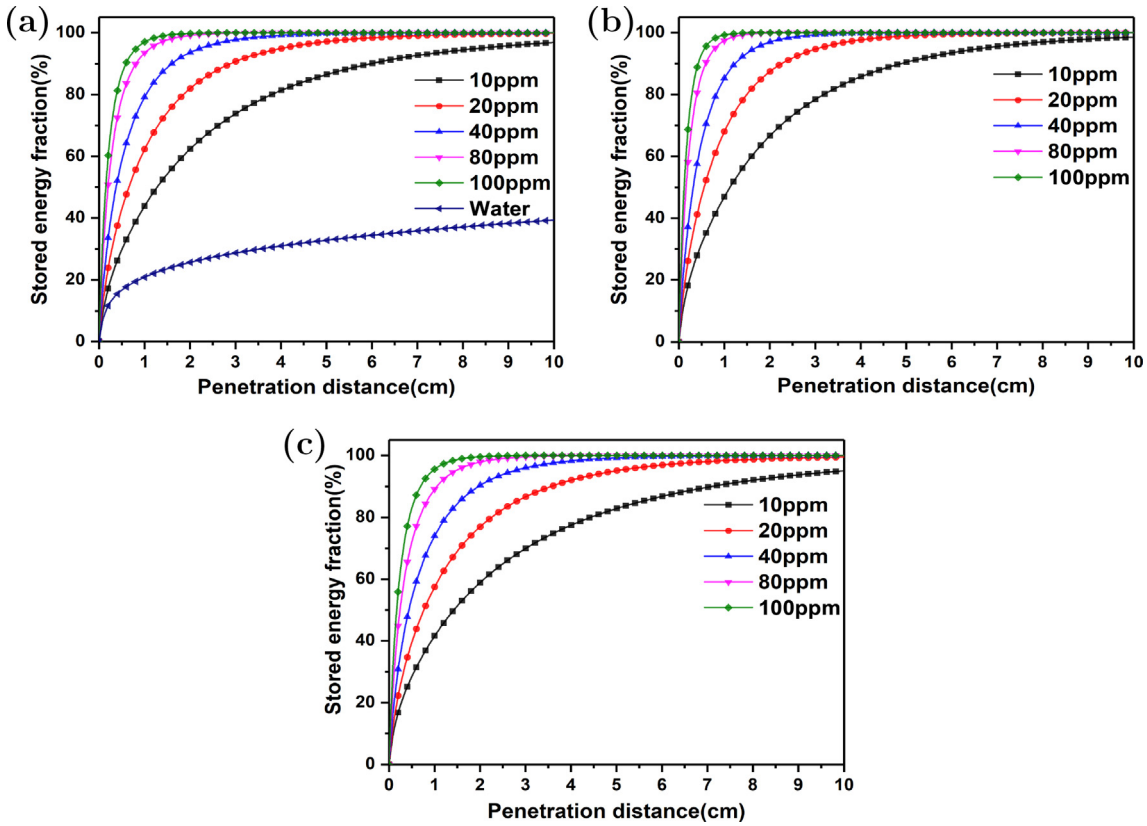

Fig. 8. Solar energy absorption fraction as a function of penetration distance for (a) Water and rGO (b) S1 (c) S2.

of about 96% in the wavelength range of 200–900 nm, while typical absorption peaks exist at 900–1000 nm and again at 1200 nm. The rGO nanofluids are more opaque above the 40 ppm in the UV wavelength range (200–400 nm). The average transmittance of the rGO nanofluids is about 80% for 10 ppm, which decreases substantially to approximately 10% for 100 ppm. The rGO nanofluids at different concentrations maintain an analogous behaviour compared with the base fluid, except the occurrence of an absorption valley around a wavelength of 270 nm due to the strong absorption of graphene.

Exploiting the LSPR, the absorption can be considerably improved for the Ag-rGO nanofluids. As shown in Fig. 6(b) and (c), a local transmittance minimum appears, centered at ~420 nm. Additionally, the transmittance of S1 reduces in the wavelength range of 500–2500 nm as compared with water. The average transmittance of the S1 nanofluids is about 76% for 10 ppm and below 5% for 100 ppm, which indicates a higher reduction of transmittance if compared with the rGO nanofluids. The decoration of Ag nanoparticles on the rGO sheets enhances their reduction ratio and electric field, shifting the absorption peak to the visible range. It is observed that a higher content of Ag in the S2 nanofluid leads to stronger absorption in the wavelength range of 400–500 nm. Although the concentration of the Ag nanoparticles in S2 is higher, the average absorption ability of these nanofluids is a slightly lower than for the rGO and the S1 nanofluids. As mentioned in Section 2, this might be explained by the fact that the overall number of the Ag-rGO nanosheets in S2 is lower than in S1 at the same mass fraction, since the density of Ag is higher than of rGO. Notably, as the particle size or concentration of the metal particles increases, scattering gradually plays a prevailing role.

The extinction coefficient $\alpha(\lambda)$ from the spectral transmittance $T(\lambda)$, can be calculated based on the Lambert-Beer law to better understand the optical properties of the nanofluids, as given below [8]

$$T(\lambda) = e^{-\alpha(\lambda)l}, \tag{1}$$

where l is the optical path length within the nanofluids, which is 10 mm in our work. The spectral extinction coefficient that phenomenologically contains the spectral absorption, including the spectral scattering, is shown in Fig. 7 for the rGO, S1 and S2 samples. It can be seen that the rGO and Ag-rGO nanofluids can considerably increase the extinction coefficient in the UV–visible region. This effect is weaker at higher wavelengths. Advantageously, the Ag-rGO nanofluids contain a broad peak at ~420 nm, which is very close to the highest intensity of the solar irradiance at 480 nm. It is can be also observed that the extinction coefficient peaks of S2 are much higher at the LSPR wavelength compared with S1 nanofluids, which gradually redshifts and produces an evident broadening due to the increase of the weight ratio of $AgNO_3$ to GO. The interplay between the suspended nanosheets can easily be influenced by the concentration. The multi-scattering rises at higher concentrations and increases the optical paths length within the nanofluid, which will enhances the absorption.

Next, the absorbed energy fraction F is calculated to assess the amount of absorbed incident radiation, which plays a key role in solar energy systems. As a matter of fact, the fraction F of the incident power that after a path length x within the sample is no more available to be transmitted and it is stored in the material (either for direct absorption or scattering followed by absorption process), is given by the expression [47]:

$$F(x) = 1 - \frac{\int_{\lambda_{min}}^{\lambda_{max}} I(\lambda) e^{-\alpha(\lambda)x}\, d\lambda}{\int_{\lambda_{min}}^{\lambda_{max}} I(\lambda)\, d\lambda}, \tag{2}$$

where $I(\lambda)$ is the solar radiation (CIE solar spectrum with AM = 1.5), $\lambda_{max} = 2500$ nm and $\lambda_{min} = 200$ nm are the maximum and minimum considered wavelengths of the solar spectrum.

Fig. 8 demonstrates the calculated absorbed energy fraction for different nanofluids as a function of penetration distance. The absorbed energy fraction for different penetration depths plays an important role in the design of DASC collectors that can provides information regarding the optimum concentration and collector height. It can be

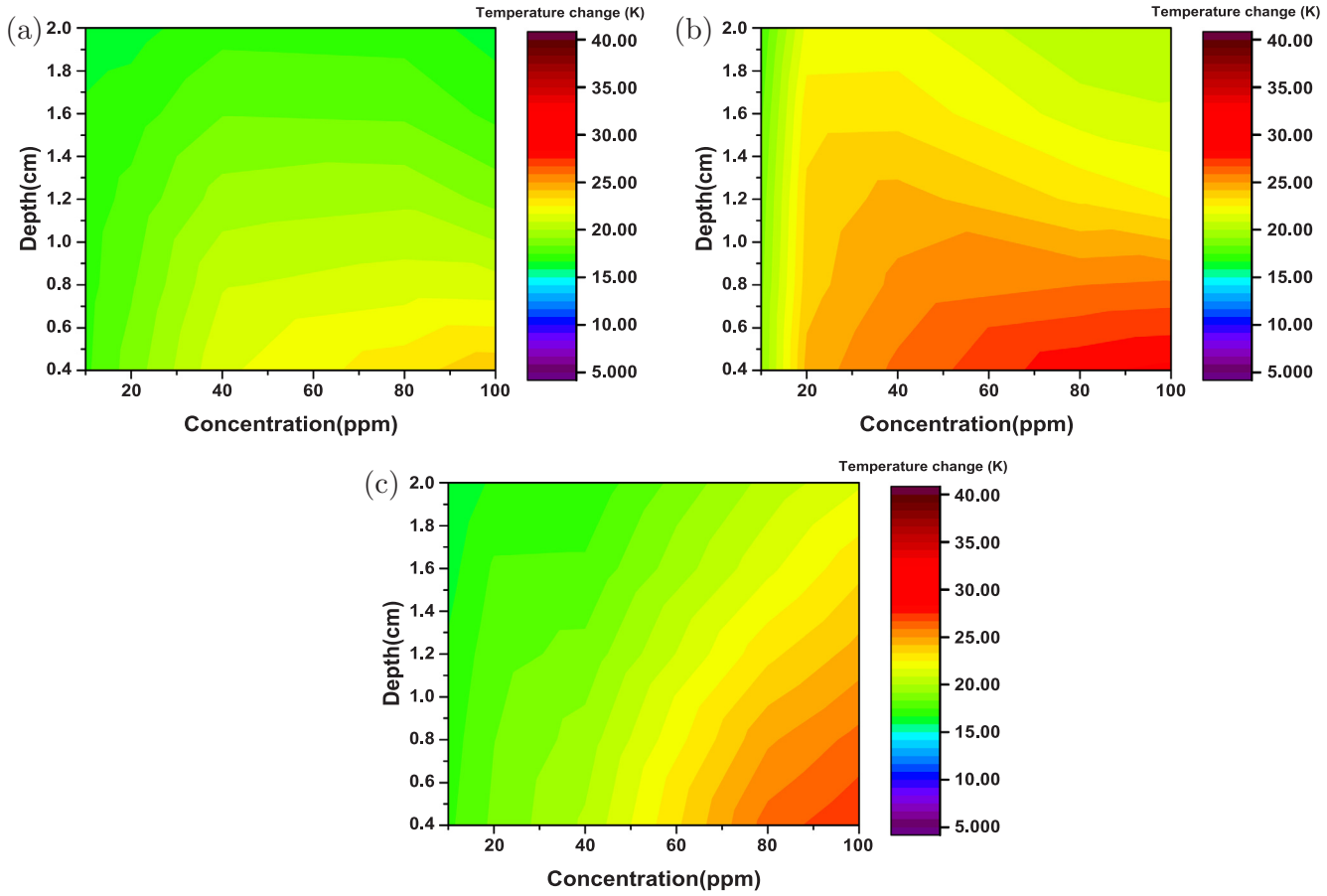

Fig. 9. Temperature profiles at different heights and concentrations for the (a) rGO (b) S1 and (c) S2 nanofluids after irradiation time of 2000 s; the top of the cylinder is at depth = 0.

observed that the absorbed energy fraction (F) of the rGO and Ag-rGO nanofluids are directly proportional to the nanosheet mass fraction that increases with the penetration depth. The absorption of all nanofluids is higher than for water ($F_{max} \simeq 40\%$), where samples with concentrations higher than 20 ppm can absorb the solar energy completely at a penetration depth of 10 cm. The penetration depths for S1, where $F > 99\%$, are lower than for rGO and S2 at the same concentrations, which shows that the absorption of the S1 nanofluids is the highest.

4. Photo-thermal conversion experiment

4.1. Temperature distributions

The working fluid in DASC systems absorbs the sunlight and converts its energy into heat to increase the fluid temperature. The temperature increase of different working fluids at given irradiation conditions (intensity and time) pertains to their optical absorption capability as well as their thermal conductivity and heat capacity. The photo-thermal conversion performance of water and the prepared nanofluids (rGO, S1 and S2) is tested in this section using a solar simulator at 1326 W/m^2 in a setup as shown in Fig. 2.

The temperature profiles at different heights as a function of time are shown in Fig. S2. The temperature of the water and all nanofluids increases during the solar irradiation. However, a higher temperature increase is observed for the nanofluids, confirming the improvement of the photo-thermal conversion performance. For example, the maximum temperature change on the top surface of the collector for the rGO, S1 and S2 nanofluids after an irradiation time of 2000 s, is measured to be about 24, 27.4 and 28.6 °C, respectively. The nanofluid temperature increases rapidly due to the low temperature difference between the liquid and the environment. Afterwards, the temperature increase slows down as the heat dissipation starts to play a role, which, after a longer time, will reach an equilibrium stage where heat losses and solar absorption are balanced. The temperature distributions after 2000 s within the sample are presented in Fig. 9.

As it can be seen from Fig. 9(a) and (b) for the rGO and S1 nanofluids, the temperature profiles are demonstrating different trends for varying concentrations. The low optical thickness of the nanofluid (rGO < 80 ppm, S1 < 40 ppm) allows to absorb the radiative energy equally. However, for higher concentrations of the rGO and S1 nanosheets, the increased optical thickness makes the volumetric receiver more closely resemble a surface absorber. The difference between the rGO and S1 nanofluids can be indicated in higher concentrations, when the Ag nanoparticles are able to concentrate the radiative energy and generate higher thermal energy in a small volume close to the top surface of the collector. For the S2 nanofluids, the temperature difference between the top and bottom of the cylinder increases with increasing nanosheet concentration.

4.2. Photo-thermal conversion efficiency

Given the temperature distributions, the photo-thermal conversion efficiency is based on two important assumptions: (1) the adiabatic condition for the bottom and cylinder walls of the container (thermally insulated), and (2) the major heat loss occurs at the top surface of the container by combined convection and radiation to the ambient atmosphere. The overall efficiency can then be calculated based on

$$\eta = \frac{h\rho c_p (T_{bulk|_{t=\Delta t}} - T_{initial})}{G\Delta t}, \quad (3)$$

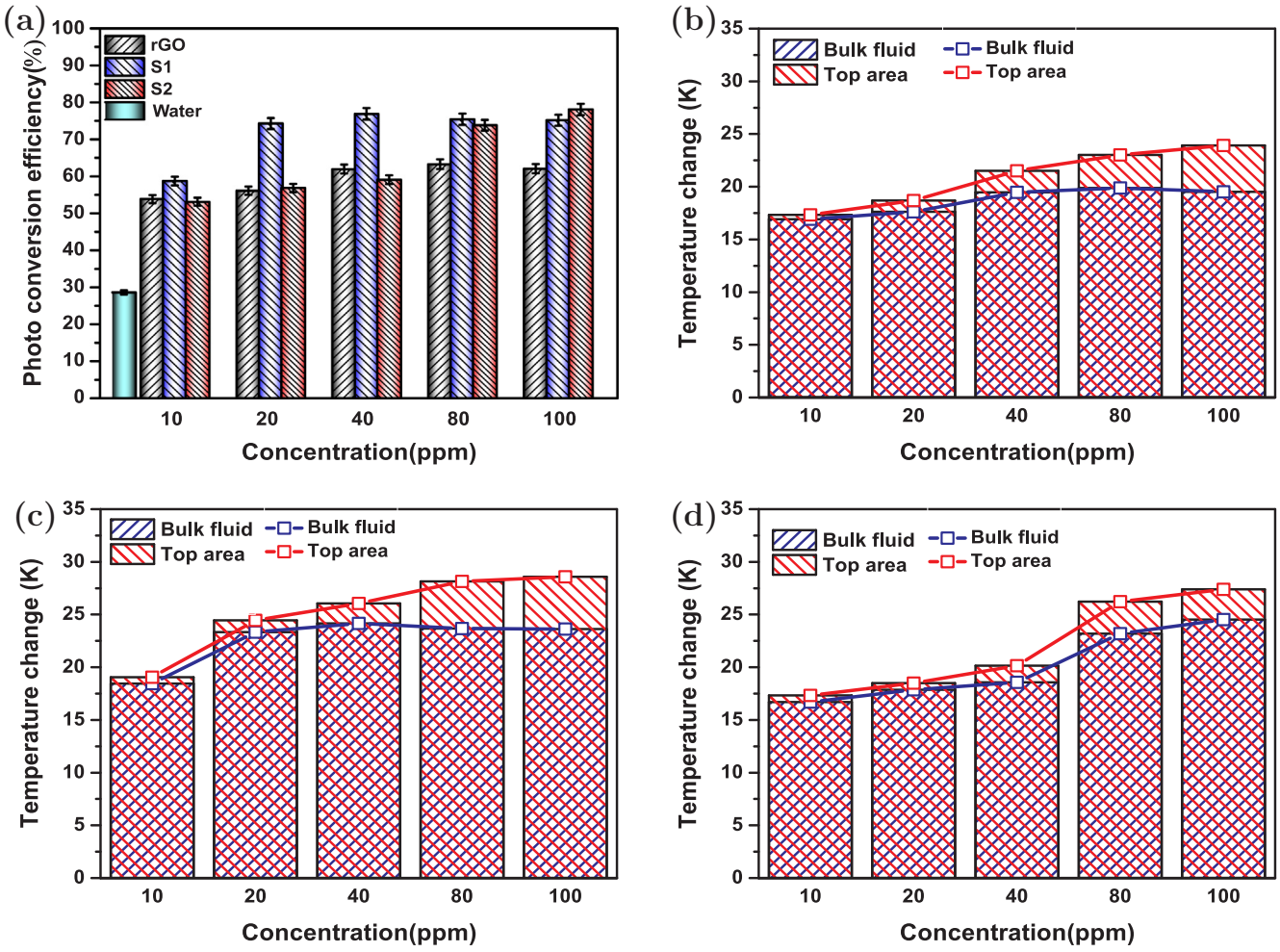

Fig. 10. (a) Collector efficiencies of water and prepared nanofluids at different concentration after light irradiation of 2000 s; top area and bulk fluid temperature of (b) rGO (c) S1 and (d) S2 nanofluids.

where ρ (kg/m^3) and c_p (J/kg K) are the density and specific heat of the water, T_{bulk} (K) is the average temperature of the fluid inside the container, $T_{initial}$ (K) is the initial temperature of the fluid, G (W/m^2) is the heat flux of the incident light from the solar simulator, t (s) is the irradiation exposure time, and h (m) is the height of the sample. In our experiment, G was measured to be about 1326 W/m^2. c_p and $\rho$of water and the nanofluids are considered to be the same, due to the relatively low concentration of nanosheets.

The photo-conversion efficiency of water and the nanofluids for a given concentration are shown in Fig. 10(a). The nanofluids have a higher overall efficiency than water due to their higher thermal conductivity and better optical absorption as discussed in the previous section. Moreover, it can be noticed that the efficiency of the collector reaches a maximum of 77% by increasing the concentration of the S1 nanofluids from 0 to 40 ppm. After further increasing the concentration, the collector efficiency decreases, since most of the radiation is captured close to the upper surface only. The same effect can be seen for the rGO nanofluid, as the maximum efficiency occurs at 80 ppm (63.3%). On the other hand, the efficiency of the S2 nanofluids reaches its maximum value (78%) at the highest concentration of 100 ppm. This can be explained by the lower particle number of Ag-rGO in S2 at a given mass fraction as discussed earlier. The bulk temperature of the fluid was calculated from an arithmetic mean of the temperature measurements at different heights to obtain more precise estimations of the overall collector efficiency. The top surface temperature (h = 0.4 cm) and the bulk temperature for different working fluids at an illumination time of 2000 s are illustrated in Fig. 10(b–d). It can be observed that the top surface temperature increased concomitantly with nanosheets concentration, while the bulk fluid temperature initially showed a different trend for different nanofluids. Simultaneously, the difference between the bulk fluid and top area temperature increased concomitantly with nanosheets concentration. The working fluid temperature distribution has a great effect on the collector performance, and it literally validates that working fluids with a high top surface temperature and a relatively low bulk temperature deliver a lower photo-thermal conversion performance.

Fig. 11(a–c) illustrates the variation of the collector efficiency corresponding to different heights and nanofluid concentrations. The local efficiency can be calculated as

$$\eta_{(y)} = \frac{h\rho c_p (T_{bulk}|_0^y - T_{initial})}{G\Delta t}, \quad (4)$$

where the bulk fluid temperature was obtained by integrating to a certain depth y.

The effect of solar collector height and nanofluid concentration on local efficiency of the collector after irradiation time of 2000 s is outlined in Fig. 11(a–c). The photo-thermal conversion performance of nanofluids is highly related to the receiver height, irradiation time, and nanoparticles concentration. The collector efficiency rapidly increases for higher concentrations and higher fluid depths due to the higher absorption of nanofluids. However, it can be seen from Fig. 11(a and b) that the collector efficiency tends to approach its maximum value, regardless of the fluid depth and nanosheets concentration for rGO and S1 samples. The S2 nanofluids can provide a higher efficiency for all

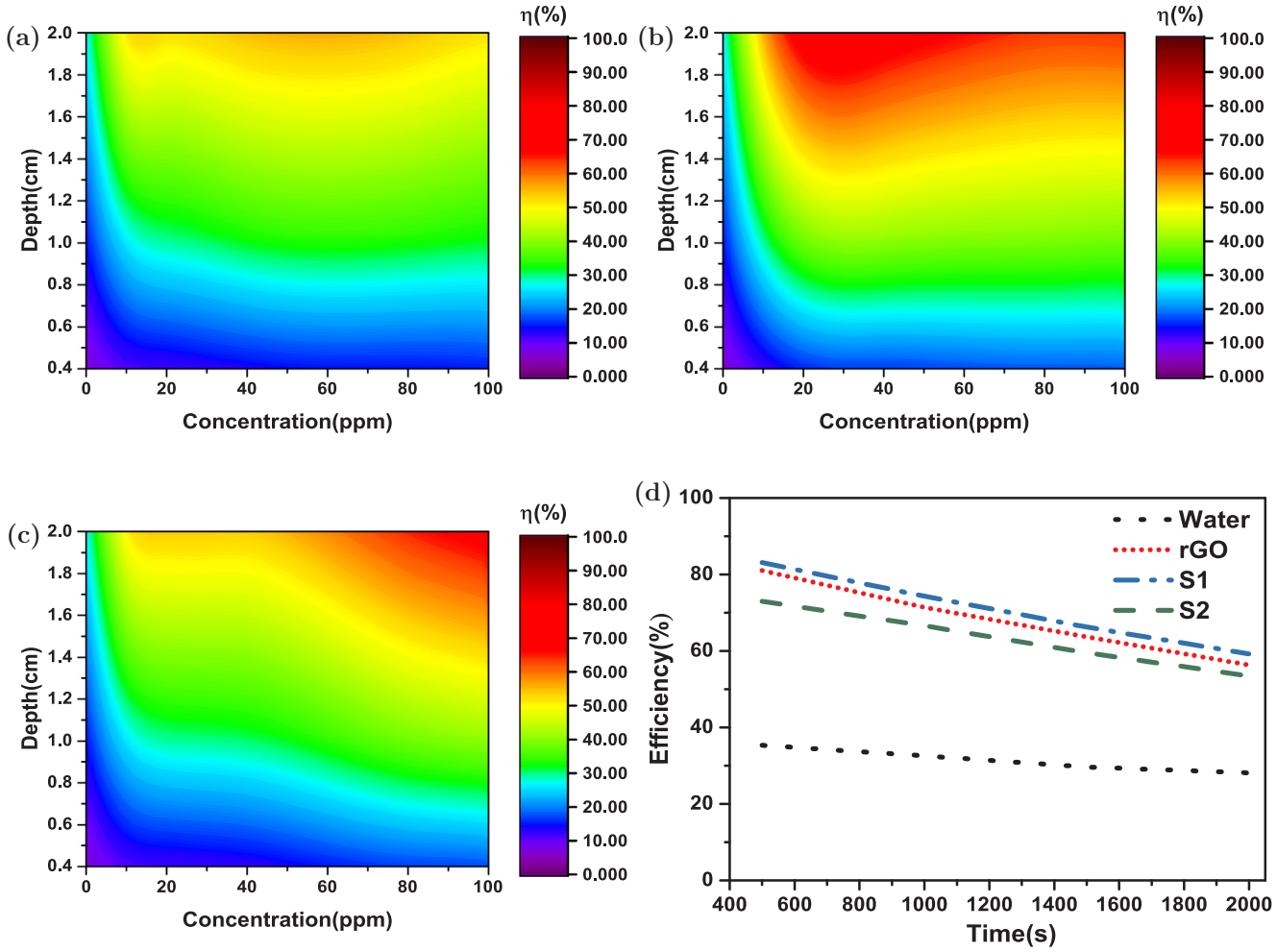

Fig. 11. Collector efficiencies as a function of collector height (h) and nanosheets concentration after irradiation time of 2000 s for (a) rGO(b) S1 and (c) S2; (d) collector efficiency as a function of irradiation time for water and nanofluids (concentration = 10 ppm and h = 20 mm).

concentrations by increasing the receiver heights (Fig. 11(c)). The S1 nanofluids can deliver a high efficiency of 76% with a low concentration of 40 ppm and a receiver height of 18 mm, while a further increase in height up to 2 cm will enhance the efficiency only by 1%.

As shown in Fig. 11(d), the irradiation time has an inverse effect on the receiver efficiency, which is associated with an increased heat loss. The efficiency decreases at a higher rate for the nanofluids if compared with water, because the equilibrium state can be reached faster. Given this fact, it is essential to choose an optimal irradiation time in terms of collector efficiency for solar energy applications. The trend in the efficiency graphs of the nanofluids suggest that a lower nanosheet concentration for the S1 samples should be considered to design efficient solar thermal collectors, since the plasmonic Ag-rGO nanofluids with a lower amount of Ag content has a favorable absorption spectrum if compared to the rGO nanofluids.

To further study and understand the effect of the Ag decoration on the photo-thermal conversion of rGO nanofluids, an IR camera was used to record the surface temperature distribution of the nanofluids (80 ppm) at an irradiation of 1 sun for 30 min. The thermal images are presented in Fig. 12 for 0, 10, 20 and 30 min of irradiation time. It is clear that the photo-thermal absorption of both S1 and S2 nanofluids were much higher compared with rGO nanofluid. The absorption of the solar energy by the nanofluid can be characterized by two main parts, which are the absorption by the bulk water and the nanoparticles absorption and scattering. The absorption efficiency of the nanofluids mainly pertain to the absorptivity of prepared nanoparticles. The transmission orientation can change when light crosses trough nanofluids which called scattering leading to the distribution of radiation intensity in different directions. The balance between absorption and scattering properties of nanofluids demonstrated significant role in their photo-thermal conversion efficiency that can be adjusted through geometry and size of nanoparticles. As illustrated in Fig. 12 and by inspecting the final average temperatures in Fig. S3, the Ag decoration on the rGO nanosheets tend to have higher absorption potency. However, the S1 nanofluids with lower Ag content show a higher photo-thermal capability due to the lower scattering effects resulting in a higher absorption.

These findings indicate the potential of these nanofluids with Ag decorated rGO nanosheets for better photo-thermal conversion performances of the DASC collectors. However, the optimized nanoparticle concentrations, as well as the collector height, should be determined based on the costs of nanoparticle and collector preparation. An optimized nanofluid can be suggested by considering three factors: (a) higher collector efficiency (b) lower nanoparticle concentration (c) lower collector height. Building on our results, to obtain a solar absorption efficiency of 77% at 1sun irradiation, the Ag-rGO (S1 sample) nanofluid with a concentration of 40 ppm and a collector height of 20 mm can be a perfect candidate for a cost effective DASC systems.

5. Conclusion

To summarize,this study demonstrated a versatile and efficient approach to prepare stable plasmonic graphene nanofluids for volumetric solar thermal energy harvesting. The unique properties of the prepared

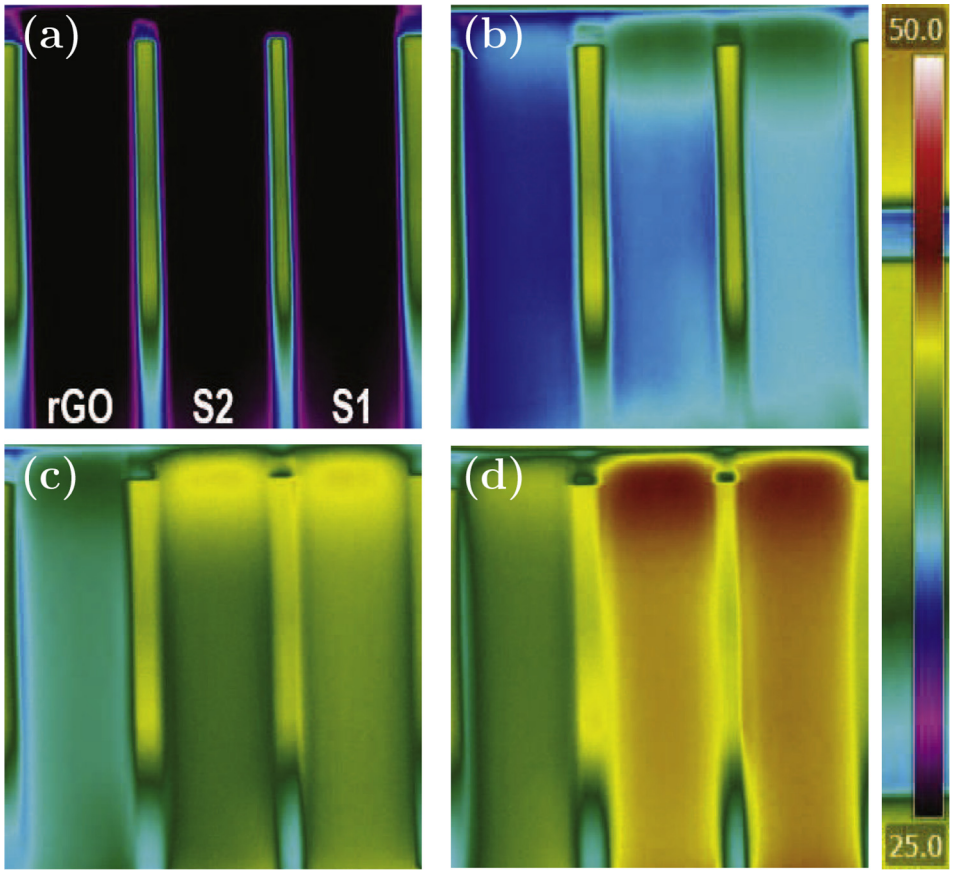

Fig. 12. IR images of 80 ppm nanofluids taken under illumination time of (a) 0 min (b) 10 min (c) 20 min and (d) 30 min.

plasmonic nanofluids can be attributed to the following major factors: (a) the decoration of Ag nanoparticles on rGO nanosheets can enhance the absorption of the incident radiation and the collective motion of electrons in Ag nanoparticles; (b) rGO nanosheets, owing to their high specific surface area and stability, can act as an ideal supporting material to avoid agglomeration of the Ag nanoparticles; (c) the photothermal potency of rGO nanofluids can be promoted by the synergistic effects between rGO and Ag nanoparticles as well as enhancement of heat transfer conduction to the surrounding base fluid (in this case water). The results indicated that the collector efficiency was significantly enhanced (2.7 times) by adding only 40 ppm of the prepared Ag-rGO nanosheets and that a realistic collector height (20 mm) can be utilized for practical applications. Further enhancements in the collector efficiency to be attained by utilizing concentrated solar radiation.

Acknowledgements

This research has received funding under Cohesion grant (P70368) from TU Delft.

Appendix A. Supplementary material

Supplementary data associated with this article can be found, in the online version, at http://dx.doi.org/10.1016/j.apenergy.2018.04.065.

References

[1] Colangelo G, Favale E, Miglietta P, de Risi A, Milanese M, Laforgia D. Experimental test of an innovative high concentration nanofluid solar collector. Appl Energy 2015;154(Suppl C):874–81.
[2] Sadeghinezhad E, Mehrali M, Rosen MA, Akhiani AR, Latibari ST, Mehrali M, et al. Experimental investigation of the effect of graphene nanofluids on heat pipe thermal performance. Appl Therm Eng 2016;100:775–87.
[3] Iranmanesh S, Ong HC, Ang BC, Sadeghinezhad E, Esmaeilzadeh A, Mehrali M. Thermal performance enhancement of an evacuated tube solar collector using graphene nanoplatelets nanofluid. J Cleaner Prod 2017;162(Suppl C):121–9.
[4] Elsheikh A, Sharshir S, Mostafa ME, Essa F, Ali MKA. Applications of nanofluids in solar energy: a review of recent advances. Renew Sustain Energy Rev 2018;82:3483–502.
[5] Mahian O, Kianifar A, Kalogirou SA, Pop I, Wongwises S. A review of the applications of nanofluids in solar energy. Int J Heat Mass Transf 2013;57(2):582–94.
[6] Amjad M, Raza G, Xin Y, Pervaiz S, Xu J, Du X, et al. Volumetric solar heating and steam generation via gold nanofluids. Appl Energy 2017;206(Suppl C):393–400.
[7] Potenza M, Milanese M, Colangelo G, de Risi A. Experimental investigation of transparent parabolic trough collector based on gas-phase nanofluid. Appl Energy 2017;203(Suppl C):560–70.
[8] Chen M, He Y, Huang J, Zhu J. Investigation into au nanofluids for solar photothermal conversion. Int J Heat Mass Transf 2017;108(Part B):1894–900.
[9] Jeon J, Park S, Lee BJ. Analysis on the performance of a flat-plate volumetric solar collector using blended plasmonic nanofluid. Sol Energy 2016;132(Suppl C):247–56.
[10] Wang X, He Y, Liu X, Cheng G, Zhu J. Solar steam generation through bio-inspired interface heating of broadband-absorbing plasmonic membranes. Appl Energy 2017;195(Suppl C):414–25.
[11] Chen M, He Y, Zhu J, Wen D. Investigating the collector efficiency of silver nanofluids based direct absorption solar collectors. Appl Energy 2016;181(Suppl C):65–74.
[12] Bandarra Filho EP, Mendoza OSH, Beicker CLL, Menezes A, Wen D. Experimental investigation of a silver nanoparticle-based direct absorption solar thermal system. Energy Convers Manage 2014;84(Suppl C):261–7.
[13] Parvin S, Nasrin R, Alim MA. Heat transfer and entropy generation through nanofluid filled direct absorption solar collector. Int J Heat Mass Transf 2014;71(Suppl C):386–95.
[14] Tyagi H, Phelan P, Prasher R. Predicted efficiency of a low-temperature nanofluid-based direct absorption solar collector. J Sol Energy Eng 2009;131(4). 041004–041004–7.
[15] Gupta HK, Agrawal GD, Mathur J. An experimental investigation of a low temperature Al_2O_3-H_2O nanofluid based direct absorption solar collector. Sol Energy 2015;118(Suppl C):390–6.
[16] Gorji TB, Ranjbar AA. A review on optical properties and application of nanofluids in direct absorption solar collectors (DASCs). Renew Sustain Energy Rev 2017;72(Suppl C):10–32.
[17] Karami M, Akhavan-Behabadi MA, Raisee Dehkordi M, Delfani S. Thermo-optical properties of copper oxide nanofluids for direct absorption of solar radiation. Sol

Energy Mater Sol Cells 2016;144(Suppl C):136–42.
[18] Gorji TB, Ranjbar AA. A numerical and experimental investigation on the performance of a low-flux direct absorption solar collector (DASC) using graphite, magnetite and silver nanofluids. Sol Energy 2016;135(Suppl C):493–505.
[19] Mu L, Zhu Q, Si L. Radiative properties of nanofluids and performance of a direct solar absorber using nanofluids. In: ASME, international conference on micro/nanoscale heat transfer, ASME 2009 second international conference on micro/nanoscale heat and mass transfer, vol. 1(43895); 2009. p. 549–53.
[20] Said Z, Sajid MH, Saidur R, Mahdiraji GA, Rahim NA. Evaluating the optical properties of TiO_2 nanofluid for a direct absorption solar collector. Numer Heat Transf Part A: Appl 2015;67(9):1010–27.
[21] Chen W, Zou C, Li X. An investigation into the thermophysical and optical properties of sic/ionic liquid nanofluid for direct absorption solar collector. Sol Energy Mater Sol Cells 2017;163(Suppl C):157–63.
[22] Shah J, Gupta SK, Sonvane Y, Davariya V. Review: enhancing efficiency of solar thermal engineering systems by thermophysical properties of a promising nanofluids. Renew Sustain Energy Rev 2017;77(Suppl C):1343–8.
[23] Ladjevardi SM, Asnaghi A, Izadkhast PS, Kashani AH. Applicability of graphite nanofluids in direct solar energy absorption. Sol Energy 2013;94(Suppl C):327–34.
[24] Karami M, Akhavan Bahabadi MA, Delfani S, Ghozatloo A. A new application of carbon nanotubes nanofluid as working fluid of low-temperature direct absorption solar collector. Sol Energy Mater Sol Cells 2014;121(Suppl C):114–8.
[25] Hordy N, Rabilloud D, Meunier J-L, Coulombe S. High temperature and long-term stability of carbon nanotube nanofluids for direct absorption solar thermal collectors. Sol Energy 2014;105(Suppl C):82–90.
[26] Wang X, He Y, Cheng G, Shi L, Liu X, Zhu J. Direct vapor generation through localized solar heating via carbon-nanotube nanofluid. Energy Convers Manage 2016;130(Suppl C):176–83.
[27] Liu J, Ye Z, Zhang L, Fang X, Zhang Z. A combined numerical and experimental study on graphene/ionic liquid nanofluid based direct absorption solar collector. Sol Energy Mater Sol Cells 2015;136(Suppl C):177–86.
[28] Ni G, Miljkovic N, Ghasemi H, Huang X, Boriskina SV, Lin C-T, Wang J, Xu Y, Rahman MM, Zhang T, Chen G, et al. Volumetric solar heating of nanofluids for direct vapor generation. Nano Energy 2015;17:290–301.
[29] Yousefi T, Veysi F, Shojaeizadeh E, Zinadini S. An experimental investigation on the effect of $Al_2O_3H_2O$ nanofluid on the efficiency of flat-plate solar collectors. Renew Energy 2012;39(1):293–8.
[30] Zhang L, Chen L, Liu J, Fang X, Zhang Z. Effect of morphology of carbon nanomaterials on thermo-physical characteristics, optical properties and photo-thermal conversion performance of nanofluids. Renew Energy 2016;99(Suppl C):888–97.
[31] Duan H, Xuan Y. Enhanced optical absorption of the plasmonic nanoshell suspension based on the solar photocatalytic hydrogen production system. Appl Energy 2014;114(Suppl C):22–9.
[32] Wang X, He Y, Liu X, Shi L, Zhu J. Investigation of photothermal heating enabled by plasmonic nanofluids for direct solar steam generation. Sol Energy 2017;157:35–46.
[33] Zhang H, Chen H-J, Du X, Wen D. Photothermal conversion characteristics of gold nanoparticle dispersions. Sol Energy 2014;100:141–7.
[34] Amjad M, Raza G, Xin Y, Pervaiz S, Xu J, Du X, et al. Volumetric solar heating and steam generation via gold nanofluids. Appl Energy 2017;206:393–400.
[35] Wang X, He Y, Liu X, Shi L, Zhu J. Investigation of photothermal heating enabled by plasmonic nanofluids for direct solar steam generation. Sol Energy 2017;157:35–46.
[36] Filho EPB, Mendoza OSH, Beicker CLL, Menezes A, Wen D. Experimental investigation of a silver nanoparticle-based direct absorption solar thermal system. Energy Convers Manage 2014;84:261–7.
[37] Raman A, Shin W, Fan S. Upper bound on the modal material loss rate in plasmonic and metamaterial systems. Phys Rev Lett 2013;110:183901.
[38] Liu T, Li D, Yang D, Jiang M. An improved seed-mediated growth method to coat complete silver shells onto silica spheres for surface-enhanced raman scattering. Colloids Surf A: Physicochem Eng Aspects 2011;387(1):17–22.
[39] Zeng J, Xuan Y. Enhanced solar thermal conversion and thermal conduction of MWCNT-SiO_2/Ag binary nanofluids. Appl Energy 2018;212:809–19.
[40] Qu J, Tian M, Han X, Zhang R, Wang Q. Photo-thermal conversion characteristics of MWCNT-H_2O nanofluids for direct solar thermal energy absorption applications. Appl Therm Eng 2017;124:486–93.
[41] Mehrali M, Tahan Latibari S, Mehrali M, Mahlia TMI, Sadeghinezhad E, Metselaar HSC. Preparation of nitrogen-doped graphene/palmitic acid shape stabilized composite phase change material with remarkable thermal properties for thermal energy storage. Appl Energy 2014;135(Suppl C):339–49.
[42] Kazi SN, Badarudin A, Zubir MNM, Ming HN, Misran M, Sadeghinezhad E, et al. Investigation on the use of graphene oxide as novel surfactant to stabilize weakly charged graphene nanoplatelets. Nanoscale Res Lett 2015;10(1):212.
[43] Raj P, Subudhi S. A review of studies using nanofluids in flat-plate and direct absorption solar collectors. Renew Sustain Energy Rev 2018;84:54–74.
[44] Sadeghinezhad E, Mehrali M, Akhiani AR, Tahan Latibari S, Dolatshahi-Pirouz A, Metselaar HSC, et al. Experimental study on heat transfer augmentation of graphene based ferrofluids in presence of magnetic field. Appl Therm Eng 2017;114(Suppl C):415–27.
[45] Dutta S, Ray C, Sarkar S, Pradhan M, Negishi Y, Pal T. Silver nanoparticle decorated reduced graphene oxide (rGO) nanosheet: a platform for sers based low-level detection of uranyl ion. ACS Appl Mater Interf 2013;5(17):8724–32.
[46] Bhunia SK, Jana NR. Reduced graphene oxide-silver nanoparticle composite as visible light photocatalyst for degradation of colorless endocrine disruptors. ACS Appl Mater Interf 2014;6(22):20085–92.
[47] Li Y, Zhao X, Zhang P, Ning J, Li J, Su Z, et al. A facile fabrication of large-scale reduced graphene oxide-silver nanoparticle hybrid film as a highly active surface-enhanced raman scattering substrate. J Mater Chem C 2015;3(16):4126–33.
[48] Azmi WH, Sharma KV, Mamat R, Najafi G, Mohamad MS. The enhancement of effective thermal conductivity and effective dynamic viscosity of nanofluids a review. Renew Sustain Energy Rev 2016;53(Suppl C):1046–58.